



# Hot deformation and processing map of GH3535 superalloy

Ya-qi JI, Shun-de QU, Wei-xin HAN

Institute of Metal Research, Chinese Academy of Sciences, Shenyang 110016, China

Received 4 December 2013; accepted 4 November 2014

**Abstract:** The hot deformation behavior of GH3535 superalloy was investigated by hot compression tests in the temperature range of 1000–1200 °C and strain rate range of 0.01–50 s<sup>-1</sup>. The activation energy is about 356.3 kJ/mol, and the flow curves and processing map were developed on the basis of experimental data. The processing map exhibits a stable domain which occurs in the strain rate range of 0.01–1 s<sup>-1</sup> at all the temperatures and a instable domain which occurs in the strain rate range of 1–50 s<sup>-1</sup>. Microstructural observations reveal that the full dynamic recrystallization (DRX) occurs in the conditions of (1150 °C, 0.01 s<sup>-1</sup>), (1200 °C, 0.01 s<sup>-1</sup>) and (1200 °C, 0.1 s<sup>-1</sup>) with different grain sizes and undissolved carbides. The flow localization and cracks occur in the regime of flow instability.

**Key words:** GH3535 alloy; hot deformation; dynamic recrystallization; carbide; processing map

## 1 Introduction

GH3535 alloy (Hastelloy N alloy) with high Mo, low Cr and C contents has excellent oxidation and corrosion resistance at high temperatures. The use of GH3535 alloy as the coolant pressure boundary limits the reactor temperature to 704 °C as GH3535 alloy softens significantly at higher temperatures [1]. For this superalloy, controlling the microstructure of the hot-worked component is very important. However, the secondary precipitates such as carbide stringers result in the difficulties in the hot working process [2]. Therefore, it is necessary to investigate the deformation behavior of this alloy to optimize the workability and control the microstructure during hot working processes.

Processing maps are developed on the basis of dynamic materials model (DMM) to represent the material response in terms of specific microstructural processes [3]. To be specific, the efficiency of power dissipation,  $\eta$ , with strain, strain rate and temperature constitutes a processing map. The parameter  $\eta$  is given as

$$\eta = \frac{2m}{m+1} \quad (1)$$

where  $m$  is the strain rate sensitivity factor, which is defined as

$$m = \left| \frac{\partial(\ln \sigma)}{\partial(\ln \dot{\epsilon})} \right|_{\epsilon, T} \quad (2)$$

On the basis of the extreme principles applied to large plastic flow body, the instability criterion is used to evaluate the regions of flow instabilities, which is expressed as

$$\xi = \frac{\partial \ln[m/(m+1)]}{\partial \ln \dot{\epsilon}} + m \leq 0 \quad (3)$$

The variation of the instability parameter with temperature and strain rate constitutes the instability map. Eventually, the superposition of the instability map on the power dissipation map constructs the processing map used to optimize hot processing parameters and control microstructure in the material.

In recent years, processing maps have been used as an available method to optimize hot working of metallic materials, such as Inconel 718, Inconel 625, Inconel 690, and Haynes 230 [4–7]. However, the studies on the deformation behavior and processing map of GH3535 alloy during hot working are few. In this work, an important guideline was provided to optimize deformation conditions and achieve the desired microstructure, and present the investigation of the hot deformation behavior and the processing map of GH3535 alloy.

## 2 Experimental

The chemical composition of the GH3535 alloy in this work is listed in Table 1. The initial microstructure of an as-received bar is shown in Fig. 1. The alloy is composed of a face-centered-cubic (FCC) austenite and molybdenum-rich  $M_6C$  carbide particles which primarily distribute at the grain boundaries. And severe mischcrystal, extremely coarse grains and a few of annealing twins exist in the initial microstructure. Isothermal compression tests were carried out on a Gleeble 3800 simulator over the temperature range of 1000–1200 °C in the step of 50 °C at the constant strain rates of 0.01, 0.1, 1, 10 and 50 s<sup>-1</sup>. The cylindrical specimens of 8 mm in diameter and 12 mm in height were machined from the bar, and long axis direction of specimens is consistent with that of the bar. Test specimens were heated to 1280 °C at the heating rate of 5 °C/s and preserved for 5 min in order to obtain the uniform grains before the compression tests. Then they

**Table 1** Chemical composition of GH3535 alloy (mass fraction, %)

C	Mo	Cr	Fe	Mn	Si	Al
0.015	17.1	7.03	4.03	0.77	0.59	0.03
W	Ti	P	S	B	Ni	
0.02	<0.01	0.004	0.001	0.0009	Bal.	

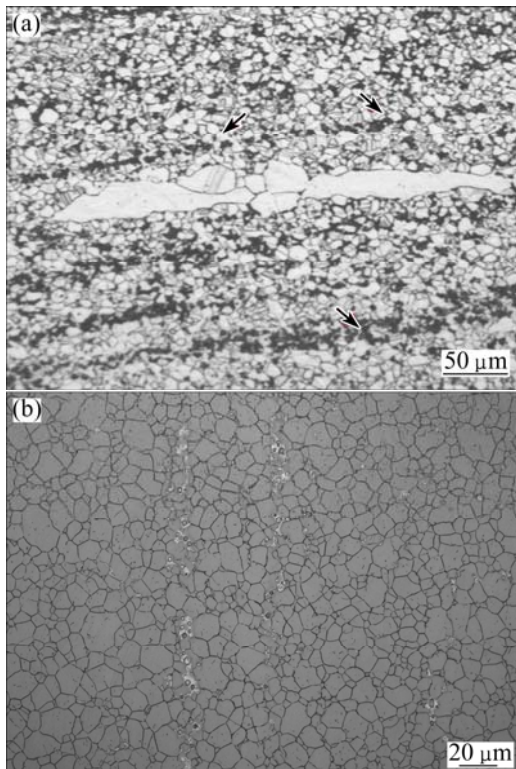


**Fig. 1** Optical microstructures of as-hot-rolled material (axial) (Arrows indicate carbide strips)

were cooled to the testing temperature and held for 3 min prior to deformation, and compressed at a true strain of about 0.7, which corresponded to the deformation degree of 50%. After hot compression, the specimens were water quenched immediately. The flow stress curves were obtained by the stress–strain data from each compression test. The deformed specimens were sectioned parallel to the compression axis for microstructure observation. The polished surfaces of the specimens were electro-etching in a 10% (mass fraction) oxalic acid aqueous solution at 4–5 V for 50–70 s.

## 3 Results and discussion

### 3.1 Flow behavior

True stress–true strain curves of the GH3535 alloys at different temperatures and different strain rates are shown in Fig. 2. It can be seen that the flow curves depend on deformation temperature and strain rate, the peak stress decreases with increasing temperature and decreasing strain rate. The work hardening stage lengthens with increasing strain rate and decreasing temperature. At low strain rate of below 1 s<sup>-1</sup>, the stress reaches the peak stress quickly and then decreases to the softening stage at lower temperatures or the steady stage at higher temperatures, which shows that the dynamic recovery and dynamic recrystallization (DRX) occur under hot deformation.

### 3.2 Kinetics analysis

The peak flow stress has a close relationship with deformation temperature and strain rate during hot deformation, which can be expressed through the Arrhenius equation as [8]

$$\dot{\varepsilon} = A[\sinh(\alpha\sigma_p)]^n \exp\left(-\frac{Q}{RT}\right) \quad (4)$$

where  $\dot{\varepsilon}$  is the strain rate;  $A$  and  $\alpha$  are material constants;  $\sigma_p$  is the peak stress;  $n$  is a parameter related to the strain rate;  $Q$  is the activation energy of deformation;  $R$  is the mole gas constant and  $T$  is the thermodynamic temperature. The value of constant  $\alpha$  is calculated as 0.0031 MPa<sup>-1</sup> and the average value of  $n$  is about 5.59. Based on the values shown in Fig. 3, the average activation energy is estimated to be about 356.3 kJ/mol. This value is greater than the self-diffusion of pure nickel ( $Q=280$  kJ/m [9]), which indicates that the DRX is the dominating mechanism in deformation procedure. The value is lower compared with the reported values of other Ni-based superalloys such as Inconel 690 (380.2 kJ/m [6]), Inconel 718 (400 kJ/m [10]) and Haynes 230 (449 kJ/m [7]). The value of constant  $A$  can be obtained as  $6.26 \times 10^{12}$  s<sup>-1</sup>. Therefore, the constitutive

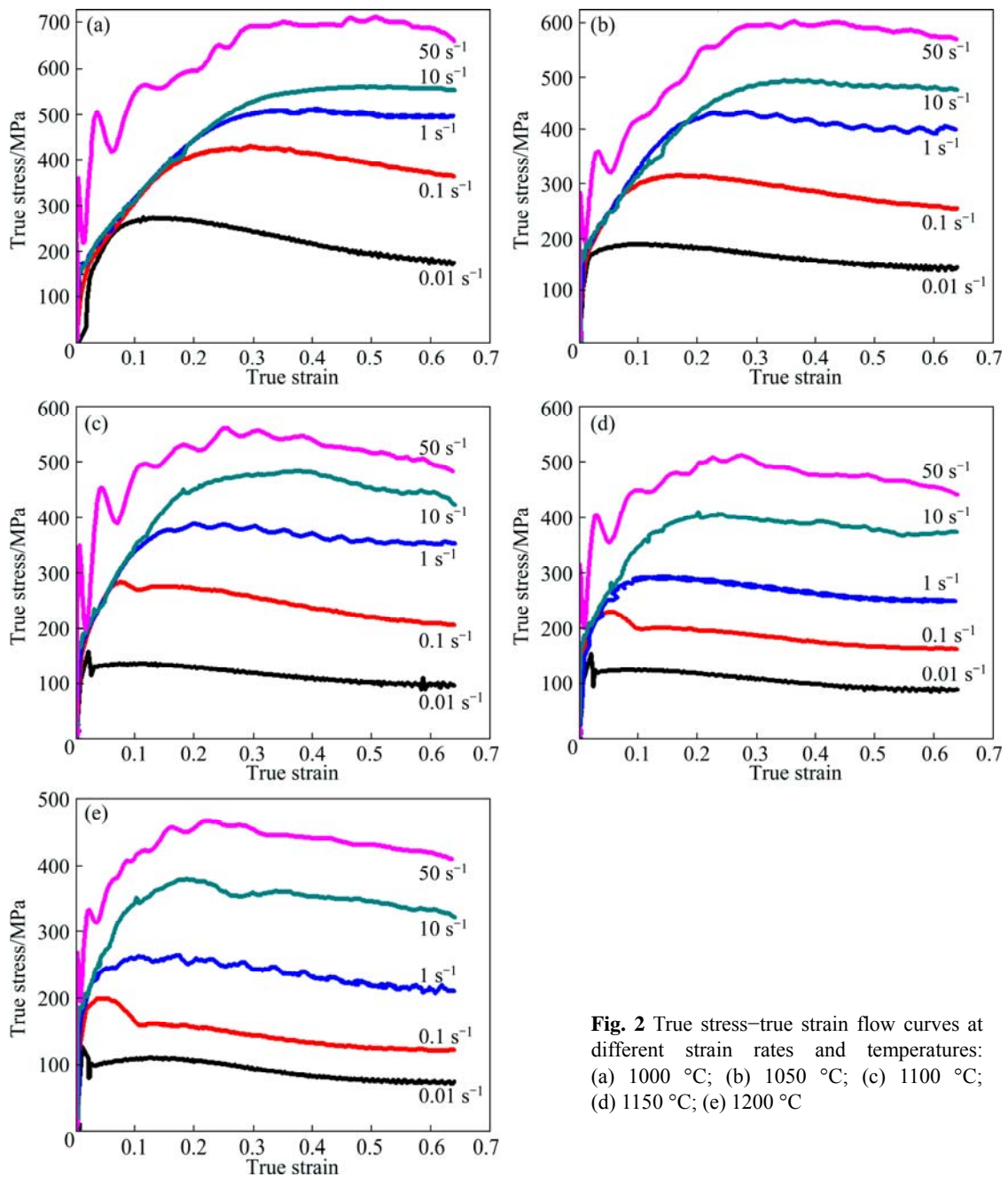


**Fig. 2** True stress–true strain flow curves at different strain rates and temperatures: (a) 1000 °C; (b) 1050 °C; (c) 1100 °C; (d) 1150 °C; (e) 1200 °C

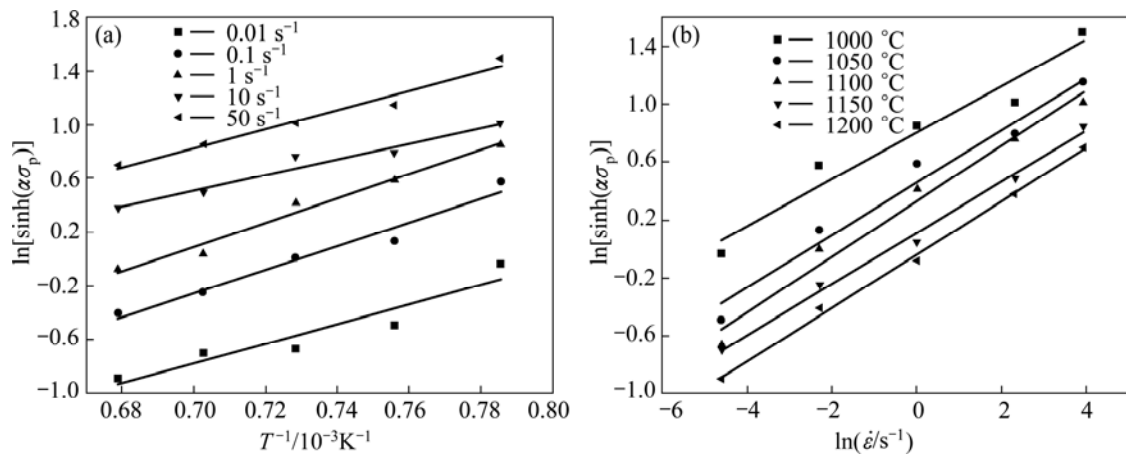


**Fig. 3** Relationship between  $\ln[\sinh(\alpha\sigma_p)]$  and different parameters: (a) Inverse of temperature; (b) Strain rate

equation of GH3535 alloy during hot deformation can be expressed as

$$\dot{\varepsilon} = 6.26 \times 10^{12} [\sinh(0.0031\sigma_p)]^{5.59} \exp\left(-\frac{356300}{RT}\right) \quad (5)$$

**3.3 Processing map**

A cubic spline at the strain of 0.6 can be obtained by interpolating all the flow stress–strain curves and correcting some data which have been affected seriously by adiabatic heating effects. The derivative of the spline fit immediately calculates the corresponding strain rate sensitivity factor *m*. The values of the efficiency of power dissipation  $\eta$  and the instability parameter  $\zeta$  can be obtained with Eq. (1) and Eq. (3) respectively. The processing map constructed by using the power dissipation map and the instability map is shown in Fig. 4. There are two main domains in the processing map of GH3535 alloy at the strain of 0.6. The first domain is located in the strain rate range of 1–50 s<sup>-1</sup> and the temperature range of 1000–1200 °C, and strain rate regimes where  $\zeta$  is negative exhibit flow instabilities. The second domain is the stable region located in the strain rate range of 0.01–1 s<sup>-1</sup> and the temperature range of 1000–1200 °C, where the dissipation efficiency increases with an increase of temperature and a decrease of strain rate. The peak efficiency of 0.44 occurs at the temperature of 1200 °C and strain rate of 0.01 s<sup>-1</sup>. As shown in the power dissipation map, the effect of strain rate on efficiency for GH3535 alloy is much greater than that of temperature.

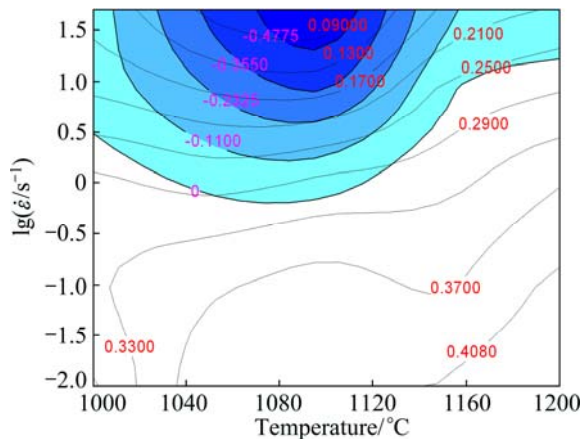


**Fig. 4** Processing map for GH3535 alloy at strain of 0.6

The typical microstructures deform under different conditions which are (1150 °C, 0.01 s<sup>-1</sup>), (1200 °C, 0.01 s<sup>-1</sup>) and (1200 °C, 0.1 s<sup>-1</sup>) in the domain where the dissipation efficiency is above 0.408, as shown in Fig. 5. The peak efficiency is 0.442 at the temperature of 1200 °C and the strain rate of 0.01 s<sup>-1</sup>. It can be observed that the uniform equiaxed grains with jagged or wavy boundaries are formed through DRX. Compared with

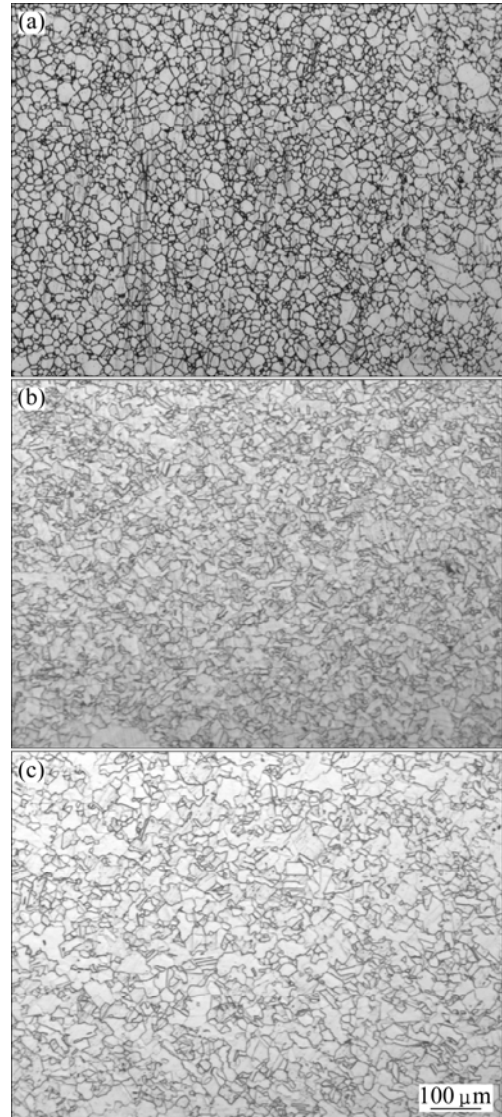


**Fig. 5** Optical microstructures of GH3535 alloy deformed to strain of 0.6 in high  $\eta$  domain: (a) 1200 °C, 0.1 s<sup>-1</sup>; (b) 1200 °C, 0.01 s<sup>-1</sup>; (c) 1150 °C, 0.01 s<sup>-1</sup>

the prior microstructures, the recrystallized structures have no stripped carbides. In addition, these microstructural observations reveal that the perfect DRX occurs in the high  $\eta$  domain. Table 2 shows the grain sizes under different conditions. It can be revealed that the grain sizes of specimens increase with increasing temperature and decreasing strain rate.

The microstructures exhibit variations of specimens in the domain with the dissipation efficiency of 0.33–

**Table 2** Grain sizes of GH3535 alloy by full DRX under different conditions

Condition	Diameter/ $\mu\text{m}$
Deformation at 1150 °C and 0.01 s <sup>-1</sup>	14.2
Deformation at 1200 °C and 0.01 s <sup>-1</sup>	29.1
Deformation at 1200 °C and 0.1 s <sup>-1</sup>	26.5

0.408 at lower temperatures and higher strain rates which are (1050 °C, 0.1 s<sup>-1</sup>), (1100 °C, 0.1 s<sup>-1</sup>), (1200 °C, 1 s<sup>-1</sup>), (1050 °C, 0.01 s<sup>-1</sup>) and (1100 °C, 0.01 s<sup>-1</sup>), as shown in Fig. 6. It is observed that the boundaries of recrystallized grains are the same as the microstructures shown in Fig. 5. There are also no stripped carbides in the recrystallization zone of deformed samples. Unlike the microstructures in the high  $\eta$  domain, these observations reveal that the process of microstructure evolution is incomplete recrystallization and the residual initial grains elongate against to the compress direction. As shown in the observation at 1050 °C, 0.1 s<sup>-1</sup>, the deformation structure is characterized by pancake-shaped original grains that are decorated with chains of ultrafine grains. The formation of new grains takes place along the original grain boundaries. The phenomenon observed can be attributed to the second phases that are still stable at hot working temperatures around 1050 °C. This also causes the restriction of the grain boundary migration [11,12]. The microstructures deform in the domain with the dissipation efficiency below 0.33, as displayed in Fig. 7. It can be demonstrated from the microstructure at

(1000 °C, 50 s<sup>-1</sup>) that cracks emerge and spread to interior of samples along the grain boundaries in the regime of flow instability. This is the reason why the flow curves shown in Fig. 2(a) begin to show a significant initial increase in the flow strength, then a continuous decrease without reaching a steady state [13]. Comparing with Fig. 6, the recrystallization zone and the new grain sizes shown in Fig. 7 are obviously smaller. This is due to no enough time or energy to grow up at the lower temperature or higher strain rate, hence flow localization emerges in the initial grains clearly.

The grain sizes and volume fraction of DRX for GH3535 alloy with the efficiency below 0.408 are shown in Table 3. The grain sizes and the volume fraction of DRX vary with different strain rates and temperatures, which is dominated by the temperature rather than the strain rate. It can be seen that the dominant mechanism of deformation is DRX in the dissipation efficiency range of 0.33–0.408, the volume fraction of DRX is over 50% in this region and the effect of soften is much greater than that of work-hardening. Below the dissipation efficiency of 0.33, the dominant mechanism

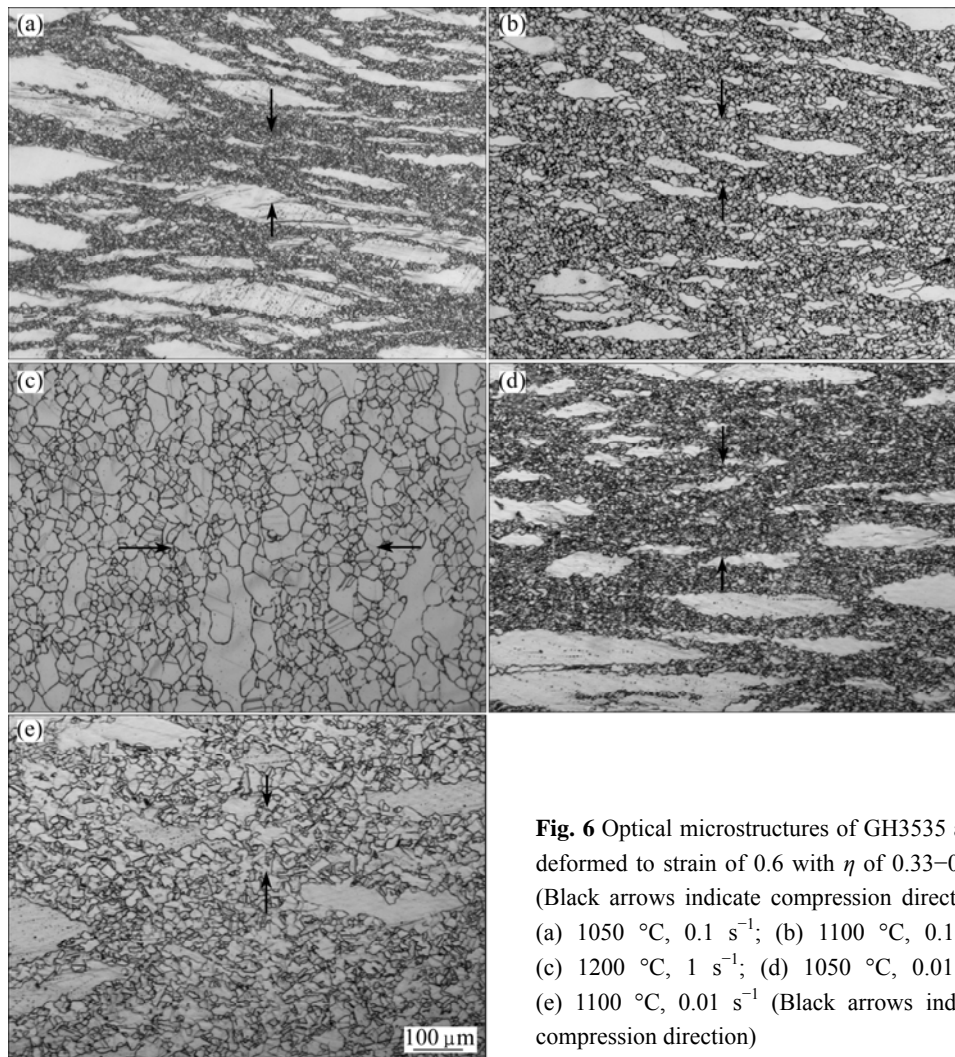


**Fig. 6** Optical microstructures of GH3535 alloy deformed to strain of 0.6 with  $\eta$  of 0.33–0.408 (Black arrows indicate compression direction): (a) 1050 °C, 0.1 s<sup>-1</sup>; (b) 1100 °C, 0.1 s<sup>-1</sup>; (c) 1200 °C, 1 s<sup>-1</sup>; (d) 1050 °C, 0.01 s<sup>-1</sup>; (e) 1100 °C, 0.01 s<sup>-1</sup> (Black arrows indicate compression direction)

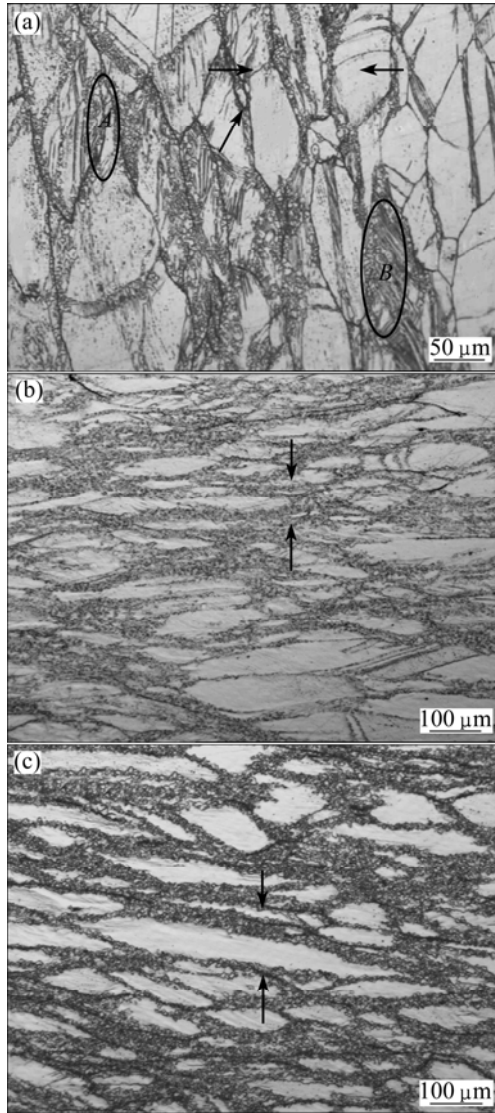


**Fig. 7** Optical microstructures of GH3535 alloy deformed to strain of 0.6 with  $\eta$  below 0.33: (a) 1000 °C, 50 s<sup>-1</sup>; (b) 1000 °C, 0.1 s<sup>-1</sup>; (c) 1000 °C, 0.01 s<sup>-1</sup> (Black arrows indicate compression direction. Red arrows indicate intergranular cracks. The areas A, B marked in (a) indicate the existence of flow localization)

**Table 3** Grain size and volume fraction of DRX of GH3535 by incomplete DRX under different conditions

Condition	Diameter of recrystallized grain/ $\mu\text{m}$	Volume fraction of DRX/%
Deformation at 1050 °C and 0.1 s <sup>-1</sup>	7.7	62.2
Deformation at 1100 °C and 0.1 s <sup>-1</sup>	11.2	83.7
Deformation at 1200 °C and 1 s <sup>-1</sup>	14.4	76.1
Deformation at 1050 °C and 0.01 s <sup>-1</sup>	11.5	73.6
Deformation at 1100 °C and 0.01 s <sup>-1</sup>	22.2	87.8
Deformation at 1000 °C and 0.01 s <sup>-1</sup>	6.7	35.7
Deformation at 1000 °C and 0.1 s <sup>-1</sup>	7.2	39.9

of deformation is dynamic recovery (DRV) and partial DRX, which means that the soften effect is equal to work-hardening effect approximately.

Based on the observations shown in Figs. 5–7, the microstructural morphology map for GH3535 alloy at a strain of 0.6 is shown in Fig. 8. Domain I is the region of perfect DRX, where the dissipation efficiency is above 0.408 and it can obtain new uniform grains at high temperatures and low strain rates. Domain II is the region of major recrystallized grains and minor slender initial grains, where the prime mechanism of deformation is same as the domain I and the dissipation efficiency is between 0.33 and 0.408. And the mechanism of hot deformation is discontinuous DRX [14,15]. Domain III is the region of vast scale slender original grains and a few new recrystallized grains, where the deformed mechanism is mainly DRV and discontinuous DRX and the dissipation efficiency is below 0.33. Domain IV is the regime of flow instability with the negative instability parameter, where dynamic recovery is the prime deformed mechanism, and intergranular cracks and flow localization exist.

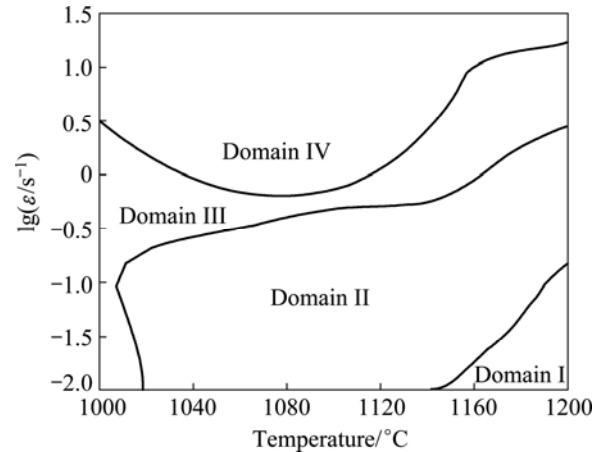


**Fig. 8** Microstructural morphology map for GH3535 alloy

### 4 Conclusions

1) The average activation energy of GH3535 alloy is calculated as 356.3 kJ/mol. The constitutive equation is expressed as

$$\dot{\epsilon} = 6.26 \times 10^{12} [\sinh(0.0031\sigma_p)]^{5.59} \exp\left(-\frac{356300}{RT}\right)$$

2) The processing map of GH3535 alloy shows two domains. The stable domain is located under the conditions of 0.01–1 s<sup>-1</sup> and 1000–1200 °C, where recrystallized microstructures replace initial grains totally or partly. The instable domain is located under the conditions of 1–50 s<sup>-1</sup> and 1000–1200 °C, where microstructural observations reveal the instability with flow localization and cracks.

3) The optimum conditions of hot working of GH3535 alloy are obtained in the temperature range of 1150–1200 °C and strain rate range of 0.01–0.1 s<sup>-1</sup>, where the perfect DRX occurs and stripped carbides dissolve in matrix crystal.

## References

- [1] HOLCOMB D E, CETINER S M, FLANAGAN G F, PERETZ F J, YODER G L. An analysis of testing requirements for fluoride salt-cooled high temperature reactor components [R]. Oak Ridge, Tennessee: Oak Ridge National Laboratory, 2009.
- [2] BRASKI D N, LEITNAKER J M. Homogenization of Ti-Hastelloy-N [J]. Metallurgical Transactions A, 1979, 10: 427–432.
- [3] CAI Da-yong, XIONG Liang-yin, LIU Wen-chang, SUN Gui-dong, YAO Mei. Development of processing maps for a Ni-based superalloy [J]. Materials Characterization, 2007, 58: 941–946.
- [4] FENG Li-sui, LI Xia-xu, LI Qing-chen, XIANG Hua-liu. Processing map for hot working of Inconel 718 alloy [J]. Journal of Materials Processing Technology, 2011, 211: 433–440.
- [5] GUO Sheng-li, LI De-fu, GUO Qing-miao, WU Zhi-gang, PENG Hai-jian, HU Jie. Investigation on hot workability characteristics of Inconel 625 superalloy using processing maps [J]. Journal of Materials Science, 2012, 47: 5867–5878.
- [6] GUO Sheng-li, LI De-fu, PEN Hai-jia, GUO Qing-miao, HU Jie. Hot deformation and processing maps of Inconel 690 superalloy [J]. Journal of Nuclear Materials, 2011, 410: 52–58.
- [7] LIU Yi, HU Rui, LI Jin-shan, KOU Hong-chao, LI Hong-wei, CHANG Hui, FU Heng-zhi. Characterization of hot deformation behavior of Haynes230 by using processing maps [J]. Journal of Materials Processing Technology, 2009, 209: 4020–4026.
- [8] SELLARS C M, MCYEGART W J. On the mechanism of hot deformation [J]. Acta Metallurgica, 1966, 14(9): 1136–1138.
- [9] THOMAS A, EL-WAHABI A, CABRERA J M, PRADO J M. High temperature deformation of Inconel 718 [J]. Journal of Materials Processing Technology, 2006, 177: 469–472.
- [10] MEDEIROS S C, PRASAD Y V R K, FRAZIER W G, SRINIVASAN R. Microstructural modeling of metadynamic recrystallization in hot working of IN718 superalloy [J]. Materials Science and Engineering A, 2000, 293: 198–207.
- [11] JIAO Shao-yang, ZHU Guan-ni, DONG Jian-xin, ZHANG Qing-quan. Carbide evolution and Mo depletion law in Hastelloy C-276 [J]. Journal of Materials Engineering, 2011(1): 47–56. (in Chinese)
- [12] AGHAIE KHAFRI M, GOLARZI N. Dynamic and metadynamic recrystallization of Hastelloy X superalloy [J]. Journal of Materials Science, 2008, 43: 3717–3724.
- [13] AMIRI A, BRUSCHI S, SADEGHI M H, BARIANI P. Investigation on hot deformation behavior of Waspaloy [J]. Materials Science and Engineering A, 2013, 562: 77–82.
- [14] WU Jie-qiong, CHEN Ke, CHEN Xing-fang, TIAN Sheng, SHEN Zhi, ZHANG Lan-ting, SHAN Ai-dang. Application of EBSD in the study of dynamic recrystallization mechanisms in nimonic 80A [J]. Journal of Chinese Electron Microscopy Society, 2011, 30(4–5): 356–359. (in Chinese)
- [15] CHEN Xing-fang, SHEN Hong-wei, CHEN Ke, WU Jie-qiong, ZHANG Lan-ting, SHAN Ai-dang. Grain structure control during hot deformation of nimonic 80A [J]. Journal of Iron and Steel Research, 2011, 23(S2): 298–301. (in Chinese)

# GH3535 合金的热变形和热加工图

季亚奇, 曲顺德, 韩维新

中国科学院 金属研究所, 沈阳 110016

**摘要:** 通过热压缩实验研究 GH3535 合金在温度区间 1000~1200 °C 和应变速率区间 0.01~50 s<sup>-1</sup> 的热变形行为。在实验数据基础上得到合金应力曲线和热加工图, 且其激活能为 356.3 kJ/mol。热加工图分为 2 个区域, 稳定区域发生在所有温度区间和应变速率区间 0.01~1 s<sup>-1</sup>, 失稳区域发生在应变速率区间 1~50 s<sup>-1</sup>。显微组织观察表明, 完全动态再结晶发生条件为(1150 °C, 0.01 s<sup>-1</sup>), (1200 °C, 0.01 s<sup>-1</sup>)和(1200 °C, 0.1 s<sup>-1</sup>), 不同条件下得到的晶粒尺寸不同且有未溶解碳化物。流变失稳区域有局部流变和裂纹出现。

**关键词:** GH3535 合金; 热变形; 动态再结晶; 碳化物; 加工图

(Edited by Xiang-qun LI)